Journal of Discovery Core
https://doi.org/10.67541/jdc2606
Research Article Volume 1, Issue 1 (July 2026) Open Access

Optimization Model for Barrier Free Accessible Routes in Community Age Friendly Environment Design Based on POI and Space Syntax

Jing Zhang *

College of Arts, Shandong Jianzhu University, Jinan, Shandong, China

***Corresponding author:** Jing Zhang. Email: outlook_8A9201AAC2554F63@outlook.com

Abstract

Aiming at the prominent problems of the spatial decoupling of road networks and functional facilities and the lack of group-differentiated quantitative support in the evaluation of barrier-free moving lines in the aging reconstruction of existing communities, this study constructs a community barrier-free accessible route evaluation and optimization model integrating point of interest (POI) data, space syntax and multi-objective optimization. Firstly, the importance weights of medical and healthcare, life service, and social leisure POIs and the Gaussian distance-decay effect are introduced into the space syntax line segment model, and the POI-weighted integration index is proposed, so that the centrality of the road structure and the attraction of facility functions can be expressed within the same framework. Secondly, based on 238 questionnaires and travel trajectory data of the elderly, a hierarchical behavioral impedance matrix was established for three groups: high-activity group, low-activity group, and wheelchair-dependent group. Walking speed, slope tolerance, continuous walking distance, and visual continuity were included in the multidimensional accessibility measurement. Furthermore, node addition, road widening, and discontinuity connection are coded as hybrid decision variables. In order to maximize POI weighted integration degree and facility coverage degree and minimize renovation cost, an improved non-dominated ranking genetic algorithm (mNSGA-II) is proposed. The demand-hierarchical Pareto ordering, spatial connectivity repair operator, and POI gravitational-field initialization strategy are introduced. The case community verification shows that the fitting coefficient of the complete model for the actual travel heat of the elderly is 0.791, which is 64.1% higher than that of the traditional space syntax model. The Pareto frontier solution set obtained by mNSGA-II improves by 43.0% and 9.1% in the inverted generational distance (IGD) and hypervolume (HV) metrics compared with the standard NSGA-II, respectively, and reduces the group payoff gap by 75.0%. After the optimization, the balanced scheme improves the POI-weighted integration degree by 18.1%, the proportion of wheelchair accessible road network by 21.2 percentage points, and the spatial fairness by 31.5%. This study provides a set of quantifiable, verifiable and traceable system optimization tools for community aging environment design.

Keywords

Design for aging environments; Barrier-free accessible routes; Point of interest data; Space syntax; Multiple objective optimization

Received: 25 Jun 2026; Revised: 20 Jul 2026; Accepted: 30 Jul 2026; Published: 19 Aug 2026

1. INTRODUCTION

This study addresses the critical gap in age-friendly community renovation by shifting the focus from isolated facility upgrades to the optimization of continuous barrier-free accessible routes.

Recognizing that existing evaluations often separate road network analysis from facility distribution and rarely account for the diverse mobility levels of older adults, this research develops an integrated framework combining POI-weighted space syntax, a hierarchical demand matrix (differentiating high-activity, low-activity, and wheelchair-dependent groups), and a multi-objective optimization algorithm. The core innovation lies in embedding facility service capacity and distance decay into spatial topology calculations, enabling the simultaneous diagnosis of two distinct problem types: "structurally convenient but facility-poor" and "facility-rich but difficult to access."

To operationalize this, the study transforms renovation actions—such as node addition, road widening, and path reconnection—into computable variables [1],[2]. An improved Pareto-based optimization is then applied to generate trade-off solutions that maximize POI-weighted integration and facility coverage while minimizing construction costs. Unlike conventional empirical or satisfaction-based approaches, this model provides a verifiable and traceable quantitative basis for decision-making [3],[4],[5].

Ultimately, the research aims not to replace designer intuition but to offer a systematic, evidence-driven tool that supports multi-objective trade-offs under budget and spatial constraints. By aligning route planning with the real travel chains and physical capacities of elderly residents, this framework facilitates a transition from piecemeal repairs to holistic network-wide optimization, ensuring that renovation efforts are both equitable and effective for all aging populations.

2.MODEL CONSTRUCTION: POI WEIGHTED SPACE SYNTAX AND MULTI-LEVEL ACCESSIBILITY MEASURE

This study adopts the segment model as the fundamental analytical unit of space syntax, as it captures the fine-grained road network characteristics within communities through angular distance while enabling the application of analytical results to specific renovation segments [6]. To balance directional continuity and actual walking length, a generalized path impedance integrating angular distance, topological steps, and metric distance is employed:

$$c_{ij} = \lambda_A \tilde{d}_{ij}^A + \lambda_T \tilde{d}_{ij}^T + \lambda_M \tilde{d}_{ij}^M \tag{1}$$

Traditional syntactic models assume homogeneous attractiveness across spatial nodes, failing to distinguish between "structurally central but facility-poor" and "facility-rich but structurally inaccessible" conditions. Therefore, POI data are introduced to enrich the model.

POI data undergo multi-source integration, deduplication, entrance matching, and age-friendly reclassification into three categories: medical and healthcare, daily services, and social leisure [7]. Weights for different elderly groups (high-activity, low-activity, wheelchair-dependent) are calibrated via the Analytic Hierarchy Process (AHP) based on travel surveys. The basic attractiveness of a single POI is defined as:

$$A_k = w_r \cdot Q_k \tag{2}$$

Where Q_k incorporates effective service intensity including facility scale and accessibility quality. Facility influences decays with increasing path impedance, using either Gaussian decay or power-law decay. The total facility received by node i is:

$$G_i = \sum_{k=1}^{K} A_k \cdot f(c_{ik}) \tag{3}$$

The POI-weighted integration (PWI) fuses spatial structure and facility gravity via a geometric weighted form:

$$PWI_i = (I_i^* + \varepsilon)^{\eta} \cdot (G_i^* + \varepsilon)^{1-\eta} \tag{4}$$

Where η controls the structural contribution coefficient. This formulation distinguishes three spatial types: structure-function dual-core segments (to be maintained as primary routes), structure-core but function-edge segments (suitable for facility supplementation), and structure-edge but function-core segments (requiring improved connectivity). For different elderly groups, path impedance must incorporate penalties for slope, curb height differences, and impassable sections, with group-specific weights w_{gr} applied in stratified PWI calculations.

Accessibility is evaluated across four hierarchical levels: topological accessibility, functional accessibility, behavioral accessibility (travel time corrected for slope, pavement, elevation differences, and rest-node spacing), and visual accessibility (visual connectivity and decision-point clarity). These four dimensions respectively address: "Is the network connected?", "Are necessary facilities available?", "Can the elderly complete the journey?", and "Is the path easy to identify?" Each level can be output independently or synthesized into a comprehensive barrier-free accessibility index (AAI). However, the composite index is used for ranking, while sub-indicators are retained for diagnosing specific shortcomings, ensuring the model identifies both overall efficiency and targeted renovation priorities.

3. OPTIMIZATION ALGORITHM: IMPROVED NSGA-II AND PARETO FRONT SOLUTION FOR BARRIER-FREE MOVING LINES

The barrier-free route renovation problem is formulated as a multi-objective combinatorial optimization on a spatial network $G_0 = (V_0, E_0, A_0)$. Candidate measures are coded as a mixed decision vector $x = (x^a, x^w, x^c)$, where $x^a \in \{0,1\}^{n_a}$ denotes node addition (rest points, ramps, accessible entrances), $x^w \in \{0,1,\dots,L_j\}^{n_w}$ denotes road widening levels, and $x^c \in \{0,1\}^{n_c}$ denotes breakpoint connections. The transformed network is $G(x) = T(G_0, x^a, x^w, x^c)$. Three core objectives are simultaneously optimized:

Maximizing POI-weighted integration:

$$F_1(x) = \frac{\sum_i q_i \cdot PWI_i\big(G(x)\big)}{\sum_i q_i} \tag{5}$$

Maximizing facility coverage:

$$F_2(x) = \frac{\sum_h p_h \sum_r w_r \, C_{hr}(x)}{\sum_h p_h} \tag{6}$$

Minimizing total renovation cost:

$$F_3(x) = C_a + C_w + C_c + C_m + C_d \tag{7}$$

Constraints include budget limits $F_3(x) \le B_{max}$, slope thresholds $s_e(x) \le s_g^{max}$, continuous walking distance limits $L_{pg}^{max}(x) \le L_g^R$, and dependency/mutual-exclusion relationships among measures.

An improved Non-dominated Sorting Genetic Algorithm (mNSGA-II) is developed with three key enhancements [8]. First, a demand-stratified Pareto strategy separates elderly groups into high-activity, low-activity, and wheelchair-dependent types, each with distinct path constraints, facility weights, and minimum improvement requirements. The scheme's minimum group benefit and group gap are defined as:

$$U_{min}(x) = min_g U_g(x) \tag{8}$$

$$Gap(x) = max_g U_g(x) - min_g U_g(x) \tag{9}$$

These are incorporated into the selection priority:

$$SP_i = \widehat{CD}_i + \lambda_u \widehat{U}_{min,i} - \lambda_g \widehat{Gap}_i \tag{10}$$

Second, a spatial connectivity repair operator identifies disconnected key nodes and greedily reconnects them using repair priority:

$$RP_k = \frac{\Delta N_k + \eta_p \Delta G_k + \eta_h \Delta H_k}{c_k^c + \varepsilon} \tag{11}$$

While also enforcing budget compliance and dependency rules. Third, population initialization is guided by POI gravitational fields, with each candidate measure's selection probability proportional to its transformation potential:

$$Pot_m = \omega_1 G_m^* + \omega_2 D_m^* + \omega_3 P_m^* + \omega_4 L_m^* \tag{12}$$

Combining random (30%), POI-guided (50%), and empirical-seed (20%) individuals to balance exploration and initial solution quality.

The algorithm dynamically couples with the space syntax model through a fitness evaluation interface. Each candidate scheme is decoded into a transformed network and submitted to Depthmap for angular segment analysis [9]. A topology hash cache avoids redundant recomputation for identical topologies:

$$H_G(x) = Hash[sort\{(u, v) \mid e_{uv} \in E(x)\}] \tag{13}$$

Different transformation operations trigger differentiated recomputation strategies: new road connections require full syntactic recalculation, while widening and rest-node additions reuse existing syntactic results and update only behavioral impedance. The overall computational complexity is reduced from $O\big(TN_P N_V (N_E + N_V \log N_V)\big)$ to:

$$O\big(T\rho N_P N_V (N_E + N_V \, log \, N_V)\big) \tag{14}$$

Through catching, approximate two-stage fitness screening, and parallel individual evaluation. Algorithm performance is evaluated against standard NSGA-II, MOPSO, and empirical baseline schemes using GD, IGD, and HV metrics [10],[11],[12]:

$$GD(P, P^*) = \left[\frac{1}{\mid P \mid} \sum\nolimits_{x \in P} d\,(x, P^*)^p\right]^{\frac{1}{p}} \tag{15}$$

$$IGD(P,P^*) = \frac{1}{|P^*|} \sum_{y \in P^*} d(y,P) \tag{16}$$

$$HV(P) = Vol\left(\bigcup_{x \in P} [F_1,(x)r_1] \times [F_2,(x)r_2] \times [F_3,(x)r_3]\right) \tag{17}$$

The reference Pareto front is constructed from aggregated non-dominated solutions across all algorithms run. Ablation experiments isolate the independent contributions of demand stratification, spatial repair, and POI-guided initialization. All stochastic runs are repeated multiple times with statistical tests (paired t-test or Wilcoxon signed-rank) to ensure significance. The comparison confirms that mNSGA-II achieves superior convergence, broader Pareto coverage, higher feasible solution rates, and more balanced accessibility gains across elderly subgroups, demonstrating its suitability for community aging renovation decisions under budget and spatial constraints.

4. EXPERIMENTAL VERIFICATION AND RESULT ANALYSIS

4.1 Selection of experimental cases and data collection

4.1.1 Principle of case community selection

Experimental cases should simultaneously satisfy the typicality of research questions, the integrity of basic data and the feasibility of optimization measures. First of all, the case should be an existing community built earlier. In the early stage of construction, such communities usually do not fully consider the continuous barrier-free travel needs of the elderly, and they are prone to problems such as insufficient road width, difference in step height, more roads at the end of the road, lack of rest nodes and difficulty in identifying facility entrances. Secondly, the aging rate of the community should be significantly higher than the average level of the city, so as to ensure that the barrier-free moving line optimization has a realistic demand. Thirdly, the road network should have a certain complexity, including main roads, branch roads and inter-building walking channels, as well as road turning points, connection interruption and uneven distribution of functional facilities, so as to test the applicability of space syntax and multi-objective optimization algorithm.

In order to reduce the subjectivity of case selection, a case suitability evaluation function consisting of the completion year, aging degree, road network complexity, barrier-free problem density and data availability is constructed:

$$S_c = \sum_{m=1}^{M} \omega_m z_{cm} \tag{18}$$

Where, S_c is the comprehensive suitability score of candidate community c; M is the number of evaluation indicators; z_{cm} is the standardized value of community c on the m-th index; ω_m is the weight of the corresponding index, and the sum of the weight is 1. For the indicator of the year of completion, the direction should be changed so that the communities with earlier completion years get higher typified scores.

This study finally selected community A as the experimental object. Built between 1988 and 1996, the community covers an area of approximately 24.6 hectares and contains 53 residential buildings and 7 primary or secondary entrances. The resident population of the community is about 6480, of which

1,917 are aged 60 and above, with an aging rate of 29.6%; There were 318 people aged 80 and above, accounting for 16.6 percent of the elderly population. The community road is composed of ring main road, group branch road and walking passage between buildings, and there are continuous slope sections, road break points and height difference obstacles locally, which has a strong representation of old communities. The basic characteristics of community A are shown in Table 1.

Table 1. A Basic characteristic of communities and typicality of cases

Indicators	Value of statistics	Judgment of characteristics
Year of establishment	From 1988 to 1996	Typical old community
Area of land	24.6 hectares	Medium scale
Permanent resident population	6,480 people	High population density
Population aged 60 and above	1,917 people	The aging rate is 29.6 percent
Number of road network segments	286 Articles	The road network structure is complex
Effective POI for the elderly	87 of them	There are many but unevenly distributed
Explicit environmental barriers	At 64	The types of barriers are diverse

It can be seen from Table 1 that the case community not only has a high proportion of elderly population but also has a complex road network and multiple types of environmental barriers. Among the 64 apparent obstacles, there are 19 elevation differences of steps or curb, 17 effective widths less than, 11 continuous slope sections, 9 road damage, and 8 difficult points of direction recognition. The above problems are not evenly distributed but mainly concentrated in the north side of the residential group, the southwest side of the activity facility entrance and some inter-building access, thus forming a difference between structural accessibility and the actual traffic capacity.

4.1.2 Data collection of community road network

The community road network data is based on the CAD base map provided by the property department, combined with on-site surveying and mapping, UAV orthophoto and manual surveying [13],[14],[15]. The CAD base map is first unified to the projection coordinate system of the study area, and the building filling, dimension marking, text description, landscape decoration line and repeated line segment are deleted, and only the road boundary, building outline, community entrance and exit, facility entrance and main public space are retained. Then the road center line is extracted according to the actual passable area, and the line segmentation is carried out at the intersection, turning point, slope change point and facility entrance.

Road network cleaning mainly includes duplicate line removal, hanging line adsorption, spurious connection exclusion and road break point correction [16]. No topological connection is established for roads that intersect geometrically but are actually blocked by walls, greening or elevation differences; For road nodes that are spatially close and confirmed to be passable on site, adsorption is carried out according to tolerance. After the cleaning, the case network contains 214 nodes and 286-line segments, with a total road length of 12.84 km and an average line length of 44.9 m.

Field measurements were made to record physical road width, actual occupied width, effective traffic width, longitudinal slope, road surface quality and elevation difference obstacles. Considering the impact of vehicle parking, facility placement and temporary piles on the net width of the road, the model uses the effective traffic width instead of the designed width [17],[18],[19],[20]:

$$b_e^{eff} = b_e^{phy} - b_e^{occ} \tag{19}$$

Where b_e^{eff} is the effective traffic width of section e; b_e^{phy} is the physical width of the road; b_e^{occ} width loss for parking, facility placement, and temporary obstacles.

The longitudinal slope of the road is calculated according to the elevation difference between the starting and ending points [21],[22]:

$$s_e = \frac{|h_e^{end} - h_e^{start}|}{l_e} \times 100\% \tag{20}$$

Where, s_e is the longitudinal slope of section e; h_e^{end} and h_e^{start} are the elevation of the end and starting point of the road section respectively; l_e is the horizontal length of the road section.

The statistical results show that the average effective width of the community road is 2.37 meters, among which the effective width of 43-line segments is less than 1.50 meters, accounting for 15.0% of all line segments; The slope of 31-line segments exceeded 5%, accounting for 10.8%; 19 Steps or large curb height differences will directly affect wheelchair access. In the common walking network, the main area of the community is basically connected; However, in the feasible network of wheelchair-dependent groups, there are two obvious breaks between the north group and the central service area.

4.1.3 POI data acquisition and on-site verification

The POI data collection range was set as an 800-meter network buffer outside the community boundary to cover peripheral medical, commercial, leisure and public transport facilities used daily by community residents. Data sources include platforms such as OpenStreetMap and AmAP, and on-site surveys are used to supplement meal assistance spots, community activity rooms, public toilets, internal fitness Spaces and rest nodes that are not included by the platforms [23].

A total of 143 POI records were obtained for the original data. After coordinating unification, name matching, category re-coding, combination of duplicate records and deletion of invalid facilities, 87 valid POIs are retained, including 18 medical and health categories, 39 life services, 21 social and leisure categories, and 9 transportation connection and emergency support categories. All facilities match the road network with physically accessible entry points, rather than directly using building center coordinates.

The effective attraction of facilities to different groups of elderly people is as follows:

$$A_{kg} = w_{rg} q_k^S q_{kg}^B q_k^O \tag{21}$$

Where A_{kg} is the effective attraction of facility k to group g; w_{rg} is the weight of group g demand for the r-th facility; q_k^S is the coefficient of facility service scale; q_{kg}^B is the accessibility availability coefficient of the facility for this group; q_k^O is the effective coefficient of opening time. The coefficients are standardized to 0-1.

The on-site verification results show that 68 of the 87 facilities can pass smoothly, accounting for

78.2%; Eleven entrances had problems such as small height difference, insufficient door width or large slope. A further eight entrances pose significant barriers for wheelchair users. Medical and health facilities are mainly distributed in the southeast side of the community, and the network distance between the residential groups on the north side and the nearest medical facilities is more than 650 meters, showing an obvious spatial supply-demand mismatch.

4.1.4 Collection of questionnaires and travel trajectories for the elderly

The questionnaire was conducted using stratified sampling by age, residential group and travel ability. A total of 268 questionnaires were distributed and 252 were returned. The survey included basic demographic attributes, daily travel purpose, frequency of facility uses, acceptable walking distance, walking speed, assistive device use, rest needs, and pair-pair comparisons of facility importance.

According to the ability to walk continuously, the degree of independence in daily activities, and the use of assistive devices, the respondents were classified as high activity, low activity, and wheelchair dependent. A total of 126 respondents participated in the simplified trajectory recording for 7 consecutive days, and 3286 valid travel trajectories were obtained after drift point cleaning, stop point identification and road matching.

The actual travel heat of the road is calculated according to the number of independent tracks per unit length:

$$H_i = \frac{n_i}{l_i} \tag{22}$$

Where H_i is the travel heat per unit length of line segment i; n_i is the number of effective active chains passing through this line segment; l_i is the length of the line segment. When the same respondent repeatedly passes the same road section in the same activity chain, it will only be counted once to avoid over-counting caused by round-trip behavior. The behavioral characteristics of the different groups are shown in Table 2.

Table 2. Samples and behavioral characteristics of the elderly with different travel abilities

Group	Number of valid samples	Average walking speed (m/s)	Average walking distance (m)	Continuous walking tolerance distance (m)	Average number of daily community trips
High vitality type	112	0.91	716	524	2.34
Low energy type	87	0.63	438	286	1.71
Wheelchair dependent type	39	0.47	267	168	1.18
Total sample	238	0.72	521	362	1.87

Table 2 shows that the average walking speed of the high-activity group is about 1.94 times that of the wheelchair-dependent group, and the continuous walking distance is about 3.12 times that of the latter. If the 500-meter walking service radius is set uniformly for all the elderly, the actual reachable range of the low-activity and wheelchair dependent groups will be significantly overestimated. Therefore, the sub-group threshold and feasible road network are used in the subsequent experiments.

4.1.5 Spatial distribution characteristics of basic data

Statistics show that 43.7% of POIs are concentrated in the southeast area, which accounts for about 22% of the total area, while the north and southwest sides account for about 38% of the residential land, but only 21.8% of the facilities for the elderly are provided. Medical and health facilities have the highest degree of agglomeration, life service facilities are relatively balanced, and social and leisure facilities are mainly distributed in the central square and the east public green space [24],[25],[26]. The imbalance degree of facilities and services is expressed by Gini coefficient:

$$G = \frac{\sum_{i=1}^{n} \sum_{j=1}^{n} | y_i - y_j |}{2n \sum_{i=1}^{n} y_i} \tag{23}$$

In the formula, G is the Gini coefficient of facility services; n is the number of residential groups; y_i and y_j are the amount of facility services obtained by the i-th and j-th groups within the acceptable impedance range, respectively. A higher value indicates a more uneven distribution of facility services.

The service Gini coefficients of medical and health care, life services and social and leisure facilities are 0.41, 0.27 and 0.34, respectively. Among them, the imbalance degree of medical services is the highest, which is basically consistent with the feedback of "long path to seek medical treatment" and "discontinuous ramp" in the questionnaire of residents in the north side.

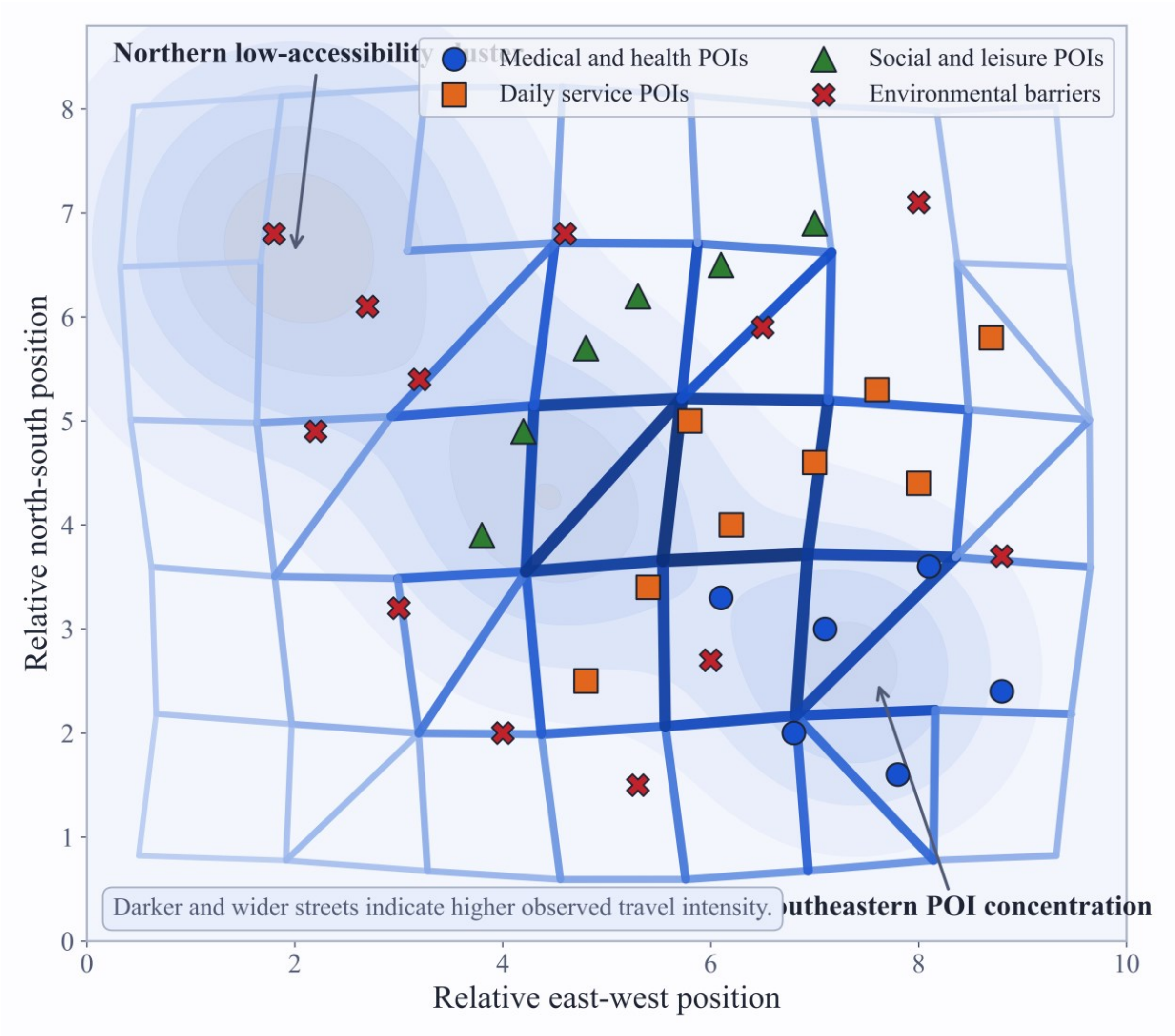

Figure 1. Distribution of POI, environmental barriers and travel trajectories of the elderly in A community

Figure 1 takes the community road network as the base map, using blue, orange and green points to represent medical and health care, life service and social leisure POI respectively, using black triangles to mark environmental obstacle points, using the width of the red line to represent the actual travel heat, and superposing the elderly population density grid. It can be seen from Figure 1 that the travel trajectory is mainly concentrated in the central ring road, the eastern entrance and exit, and the agglomeration belt of life service facilities. The cluster on the north side has a higher population density, but the actual track heat leading to the central service area is low, indicating that the low heat in this area is not entirely due to insufficient demand, but may be related to the slope, steps and path detour.

4.2 Experimental setup and parameter configuration

4.2.1 Space syntax analysis parameters

The line segment model was used in the space syntax experiment, and 300 m, 500 m, 800 m and global angle radius were set respectively. The 300-meter radius is used to describe the neighborhood activities of groups with weak mobility, the 500-meter radius corresponds to high-frequency life and travel within the community, the 800-meter radius covers cross-group activities and facilities outside the community boundary, and the global radius is used to judge the overall road structure. The topological radius was set to three levels of 3-step, 5-step, and global to compare the difference in the interpretation of angular distance with the number of topological steps.

The parameter combinations were screened by 5-fold spatial cross validation. Different from randomly dividing the road samples, the experiment divides the training set and the validation set according to the spatial grouping to reduce the accuracy overestimation caused by the spatial autocorrelation of adjacent roads. The average verification error of parameter combination q is:

$$CV_q = \frac{1}{K}\sum_{k=1}^{K} MAE_{qk} \tag{24}$$

Where, CV_q is the cross-validation error of parameter combination q; K is the number of cross-validation folds; MAE_{qk} is the mean absolute error of this parameter combination on the k-th validation set. The results for each parameter combination are shown in Table 3.

Table 3. Cross-validation results of space syntax radius parameters

Combination of parameters	Corresponding spatial scale	The validation set R^2	MAE
The angle radius is 300 meters	Neighborhood short distance activities	0.681	0.098
The angle radius is 500 meters	Community high-frequency life travel	0.742	0.083
The angle radius is 800 meters	Travel across groups and peripheral facilities	0.713	0.089
Topological radius 3 steps	Local road conversion	0.604	0.116
Topology radius 5 steps	Mesoscale topological relationships	0.636	0.108
Radius of global	Overall road network centrality	0.587	0.121

It can be seen from Table 3 that the overall fitting effect of the 500-meter angle radius is the best, and the R^2 of the validation set is 0.742, and the MAE is 0.083. The 300 m angle radius has a strong explanatory power for low activity and wheelchair dependent groups. Therefore, the 500-meter angle radius was used as the main parameter of the overall model in the experiment, and the 300-meter and 800-meter results were used for sub-group and multi-scale tests.

4.2.2 Calibration of POI gravity and behavior parameters

POI weights were obtained through the AHP judgment matrix of 238 valid questionnaires. The consistency ratios of the three types of group judgment matrices are 0.073, 0.061 and 0.058 respectively, which are all lower than 0.10 and meet the consistency requirements. By grid search and cross-validation, the Gaussian semi-decay distances of medical health, life services and social leisure facilities were determined to be 420 m, 310 m and 580 m, respectively. The corresponding attenuation coefficient is:

$$\beta_r = \frac{ln\,2}{d_{0.5,r}^2} \tag{25}$$

In the formula, β_r is the Gaussian attenuation coefficient of the r-th type of facility; $d_{0.5,r}$ is the network distance when the gravity of such facilities is reduced to 50% of the initial value. When kilometers are used as the distance unit, the attenuation coefficients of the three types of facilities are about 3.93, 7.21 and 2.06 respectively. The decline rate of living service facilities is the fastest, indicating that high frequency services such as wet market, meal aid and public toilet have strong adjacent demand; The relatively slow rate of decay of social leisure facilities indicates that some elderly people are willing to bear longer travel distances for parks, plazas and activity centers.

4.2.3 Optimization algorithm parameters

mNSGA-II, standard NSGA-II and MOPSO all set 120 individuals or particles, and the maximum number of iterations is 300 generations, with each algorithm running 30 times independently. The crossover probability is 0.90 for both mNSGA-II and standard NSGA-II, and the base mutation probability is set to the inverse of the number of decision variables. In order to avoid premature convergence in the later stage of the algorithm, mNSGA-II dynamically adjusts the mutation probability according to the population diversity:

$$p_m^t = min[p_m^{max}, p_m^0\left(1 + \eta_m \frac{D_0 - D_t}{D_0 + \varepsilon}\right)] \tag{26}$$

Where, p_m^t is the mutation probability of generation t; p_m^0 is the basic mutation probability; $p_m^{\max}$ is the upper limit of mutation probability; D_t is the population diversity of generation t; D_0 is the initial diversity; η_m is the adjustment coefficient.

The MOPSO external file capacity is 150, and the inertia weight decreases linearly from 0.90 to 0.40. The three algorithms use the same objective function, library of candidate measures, budget constraints, and random seed sets.

Table 4. Parameter configuration of the optimization algorithm

Parameters	mNSGA-II	Standard NSGA-II	MOPSO
Population or particle size	120	120	120
Maximum number of iterations	300	300	300
Number of independent runs	30	30	30
Probability of crossing	0.90	0.90	—
Base mutation probability	$1/n$	$1/n$	Position disturbance 0.10
External file capacity	—	—	150
Stability judgment window	Generation 20	Generation 20	Generation 20

In order to ensure fairness, the algorithm comparison not only controls the iteration times, but also records the exact space syntax evaluation times. If only algebra is compared, mNSGA-II using caching and constraint repair may have different actual computational burden from the comparison algorithm, thus affecting the interpretation of results.

4.2.4 Software and hardware environment

CAD base map cleaning is done in AutoCAD, coordinate processing, POI matching and spatial visualization using QGIS. DepthmapX is used for space syntax line segment analysis, population evolution, topology update, POI gravity calculation, cache management and statistical test are implemented in Python, and MOPSO results are reviewed in MATLAB.

The experiment was run on a 64-bit workstation with a 16-core processor and 64 GB of memory. The space syntax task uses eight parallel processes, each configured with its own temporary directory. Random seeds, network versions, parameter files, cache hit records, and final non-dominated solutions are saved in each run to ensure that the experiment can be reproduced.

4.3 Verification of POI weighted space syntax model

4.3.1 Verification method and evaluation index

In model validation, the actual road travel heat was used as the dependent variable, and the traditional topological integration degree, traditional angle integration degree, POI weighted integration degree and full multi-level accessibility model were successively used as explanatory models. The coefficient of determination is used to measure the degree to which the model explains the actual difference in heat:

$$R^2 = 1 - \frac{\sum_{i=1}^{n}(y_i - \hat{y}_i)^2}{\sum_{i=1}^{n}(y_i - \bar{y})^2} \tag{27}$$

Where R^2 is the coefficient of determination; y_i is the actual travel heat of road i; $\hat{y}_i$ is the prediction heat of the model; $\bar{y}$ is the average value of actual heat; n is the number of road samples [27], [28], [29], [30].

The meaning of absolute error is [31], [32], [33], [34], [35]:

$$MAE = \frac{1}{n}\sum_{i=1}^{n} | y_i - \hat{y}_i | \tag{28}$$

Both actual and predicted heat are standardized to 0-1, so a lower MAE indicates a more accurate model prediction, [36], [37], [38], [39].

4.3.2 Comparison between weighted model and traditional model

The validation results of the four types of models are shown in Table 5.

Table 5. Fitting results of different models for the actual travel heat of the elderly

Model	Core variable	R^2	MAE	MAE reduction relative to the topological model
Traditional topological integration model	Integration degree of topological steps	0.482	0.137	—
Traditional angle integration degree model	500 m angle integration	0.598	0.112	18.2%
POI weighted integration degree model	Degree of angular integration and facility gravity	0.742	0.083	39.4%
Full multi-level model	Weighted integration, behavior, and visual modification	0.791	0.071	48.2%

The traditional topology model explained only 48.2% of the variance in road heat. After the angular distance is adopted, R^2 increases to 0.598, indicating that the path choice of the elderly is not only related to the number of transitions, but also affected by the turning angle and direction continuity. After the introduction of POI facility gravity, R^2 increases to 0.742, and MAE decreases to 0.083, indicating that facility type, use importance and distance attenuation can explain a large number of travel activities that cannot be explained by pure spatial topology.

The slope, effective width, height difference, rest condition and visual continuity were further added to the full model, and R^2 reached 0.791, which was 0.049 higher than that of the POI weighted model. It can be seen that POI weighting is the main source of model accuracy improvement, while behavioral and visual modification can explain the actual heat decline caused by local obstacles.

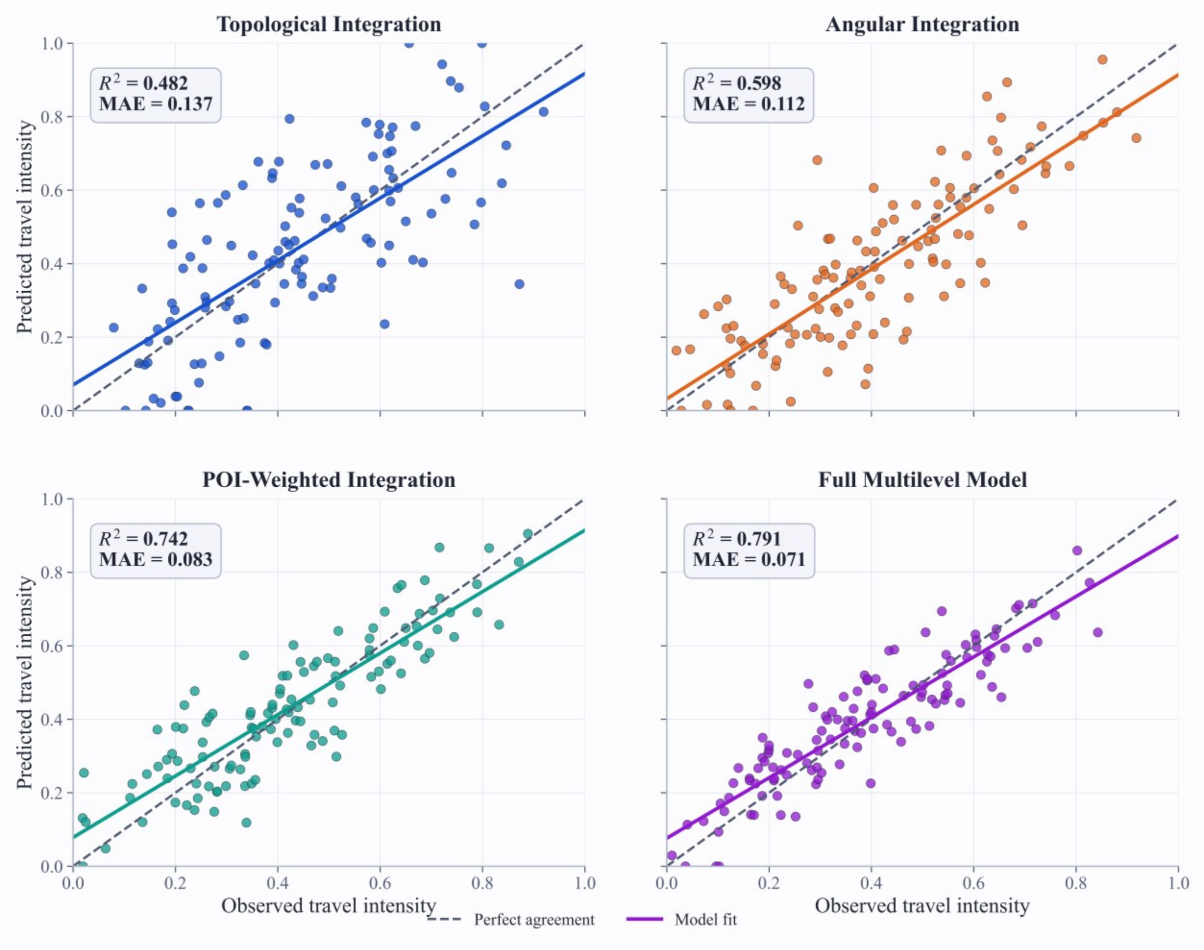

Figure 2. Scatter plot of the fit between the predicted heat of different models and the actual travel heat

Figure 2 consists of four subplots, with standardized actual heat on the horizontal axis and standardized predicted heat on the vertical axis, and a 45° reference line is plotted. The dispersion degree of the traditional topology model is high, and the heat of the facility connection section is obviously underestimated. The scatter of the POI-weighted model is closer to the reference line; The full model further reduces the prediction bias of the ramp road segment and the height difference obstacle segment.

4.3.3 Hierarchical verification of different travel ability groups

The three groups were validated using corresponding trajectories, facility weights, and behavioral parameters, respectively, and the results are shown in Table 6.

Table 6. Model fitting results for different groups of elderly people

Group	Model of angle R^2	POI weighted model R^2	The complete model R^2	The complete model MAE
High vitality type	0.641	0.758	0.781	0.068
Low energy type	0.554	0.731	0.804	0.073
Wheelchair dependent type	0.419	0.662	0.776	0.079
Total sample	0.598	0.742	0.791	0.071

The high-activity group has a strong path adaptability, and the traditional perspective model can explain 64.1% of the difference in heat. The low-activity and wheelchair dependent groups were more sensitive to slope, steps, road width, and continuous rest conditions, so the fit of the traditional model was significantly lower. After the group behavior modification is added, the R^2 of the wheelchair-dependent group increases from 0.662 to 0.776, indicating that the feasible road network of the sub-group is more in line with the actual activity conditions than the unified road network.

The MAE of the wheelchair-dependent group is still slightly higher than that of the other groups, which may be mainly related to the relatively limited sample size, the time fluctuation of temporary parking, and the fact that the path preference of escorts is not fully incorporated into the model.

4.3.4 Spatial superposition of thermal map and actual trajectory

The model predicted value and the actual trajectory heat are divided into five levels. If the difference between the predicted grade and the actual grade of a road is not more than one level, it is judged as a spatial match. The matching rate of spatial level is:

$$SMR = \frac{N_{|\Delta L| \leq 1}}{N} \times 100\% \tag{29}$$

In the formula, SMR is the spatial level matching rate; $N_{|\Delta L| \leq 1}$ is the number of roads whose difference between the predicted grade and the actual grade is less than one grade; N is the total number of roads.

The spatial matching rate of the POI weighted model is 83.6%, and that of the traditional angle model is 68.2%, an increase of 15.4 percentage points.

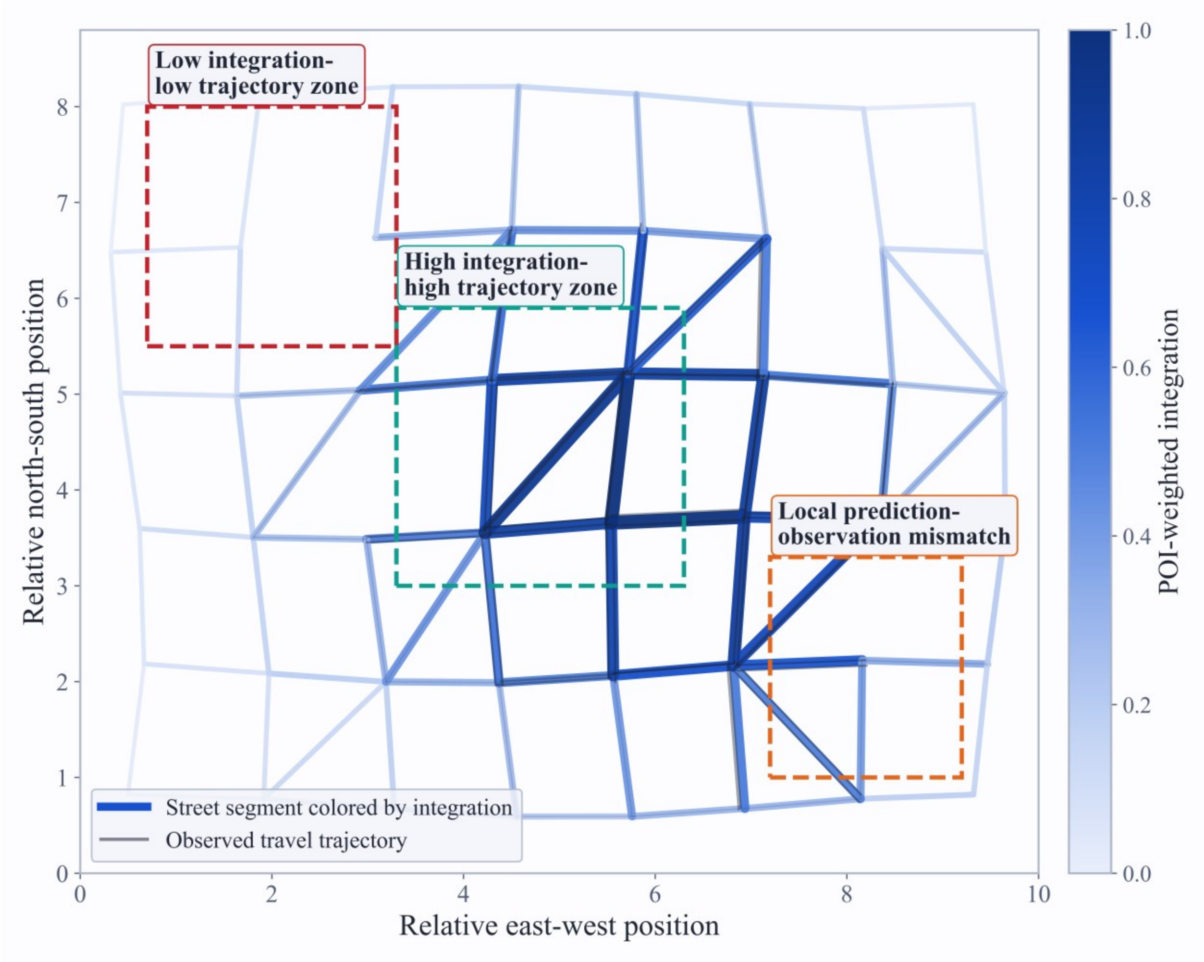

Figure 3. Thermal map of POI weighted integration degree and superposition of actual trajectory

Figure 3 shows the POI weighted integration degree with blue, red gradient, and superposes the translucent black actual trajectory. The central loop and the east service belt are consistent areas of "high integration and high trajectory". The north side of the ramp shows a consistent area of "low integration and low trajectory". There is a local deviation of "higher predicted, lower actual" near the entrance of the activity room on the southwest side. On-site review shows that the entrance is often occupied by motor vehicles at noon, indicating that the model has a good ability to explain stable spatial conditions, but it is still insufficient for temporary parking and dynamic opening of facilities.

4.4 Performance evaluation of the optimization algorithm

4.4.1 Convergence analysis of GD and IGD

The three algorithms are run independently 30 times, and the non-dominated solutions obtained from all the runs are merged and the non-dominated set is extracted again to construct the empirical reference Pareto front. The average GD of generation t is:

$$\bar{GD}_t = \frac{1}{R}\sum_{r=1}^{R} G\,D_{tr} \tag{30}$$

In the formula, $\bar{GD}_t$ is the average GD of generation t; R is the number of independent runs;

GD_{tr} is the GD value of the r-th run in generation t. The final results are shown in Table 7.

Table 7. **Comprehensive performance comparison of the three algorithms**

Algorithm	GD	IGD	HV	Feasible solution ratio	Average running time
mNSGA-II	0.0187	0.0249	0.781	96.4%	46.8 min
Standard NSGA-II	0.0328	0.0437	0.716	71.3%	52.5 min
MOPSO	0.0396	0.0518	0.684	75.8%	49.7 min

Compared with standard NSGA-II, the GD and IGD of mNSGA-II are reduced by about 43.0%, HV is increased by 9.1%, and the feasible solution rate is increased by 25.1 percentage points. Compared with MOPSO, GD and IGD of mNSGA-II were reduced by 52.8% and 51.9% respectively. The results show that the solution set obtained by the improved algorithm is closer to the empirical reference frontier and has better target space coverage ability.

Although mNSGA-II adds hierarchical sorting and repair operations, the average running time is shorter. In the experiment, the topology cache hit ratio is 34.7%, and the number of complete syntactic calls is 27.9% less than that of standard NSGA-II, which offsets the time cost caused by the new sorting and repair process.

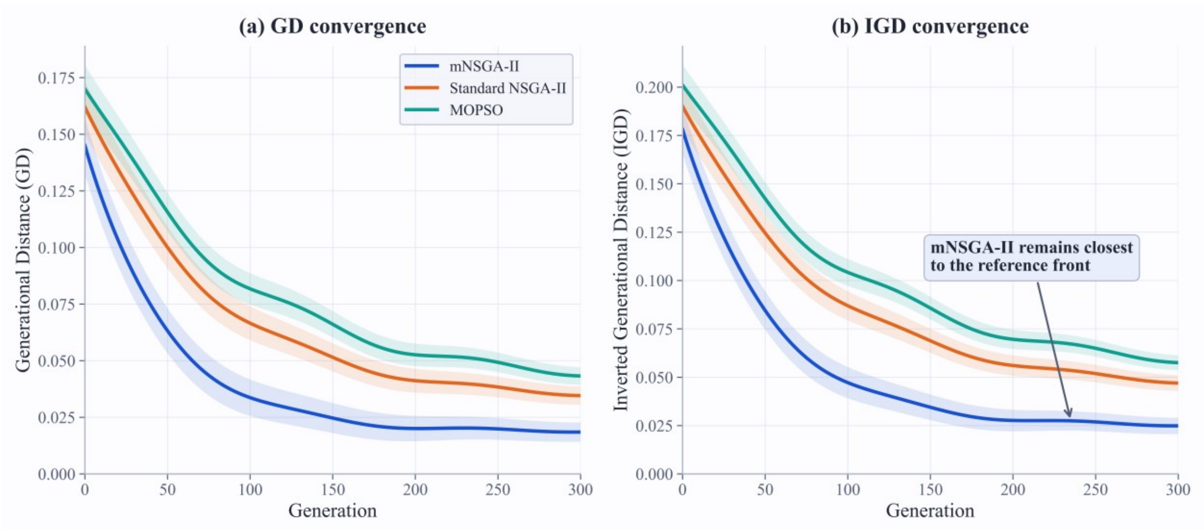

Figure 4. **GD and IGD iteration curves of the three algorithms**

Figure 4 plots the GD and IGD means of the three algorithms in 300 generations, respectively, with 95% confidence intervals indicated by shadows. mNSGA-II decreases the fastest in the first 50 generations, which indicates that POI gravity initialization can improve the quality of the initial scheme. After about 160 generations, the improvement rate of standard NSGA-II slowed down obviously, while mNSGA-II still maintained a steady decline. MOPSO fluctuates obviously in the later stage, which indicates that complex discrete constraints have a certain impact on particle position updates.

4.4.2 Pareto frontier and solution set diversity

The 3D Pareto frontier takes the transformation cost, POI weighted integration improvement rate and facility coverage improvement rate as coordinates. mNSGA-II eventually obtained 74 non-dominated schemes, while standard NSGA-II and MOPSO obtained 51 and 46 schemes, respectively. The uniformity of solution set distribution is evaluated by spacing index:

$$SP = \sqrt{\frac{1}{N_P - 1}\sum_{i=1}^{N_P}(\bar{d} - d_i)^2} \tag{31}$$

In the formula, SP is the spacing index; N_P is the number of non-dominated solutions; d_i is the distance between scheme i and its nearest neighboring scheme; $\bar{d}$ is the average value of nearest neighboring distance. The smaller the value, the more evenly distributed the solution set.

The spacing indices of mNSGA-II, standard NSGA-II and MOPSO are 0.021, 0.037 and 0.044, respectively, indicating that mNSGA-II has better solution set diversity.

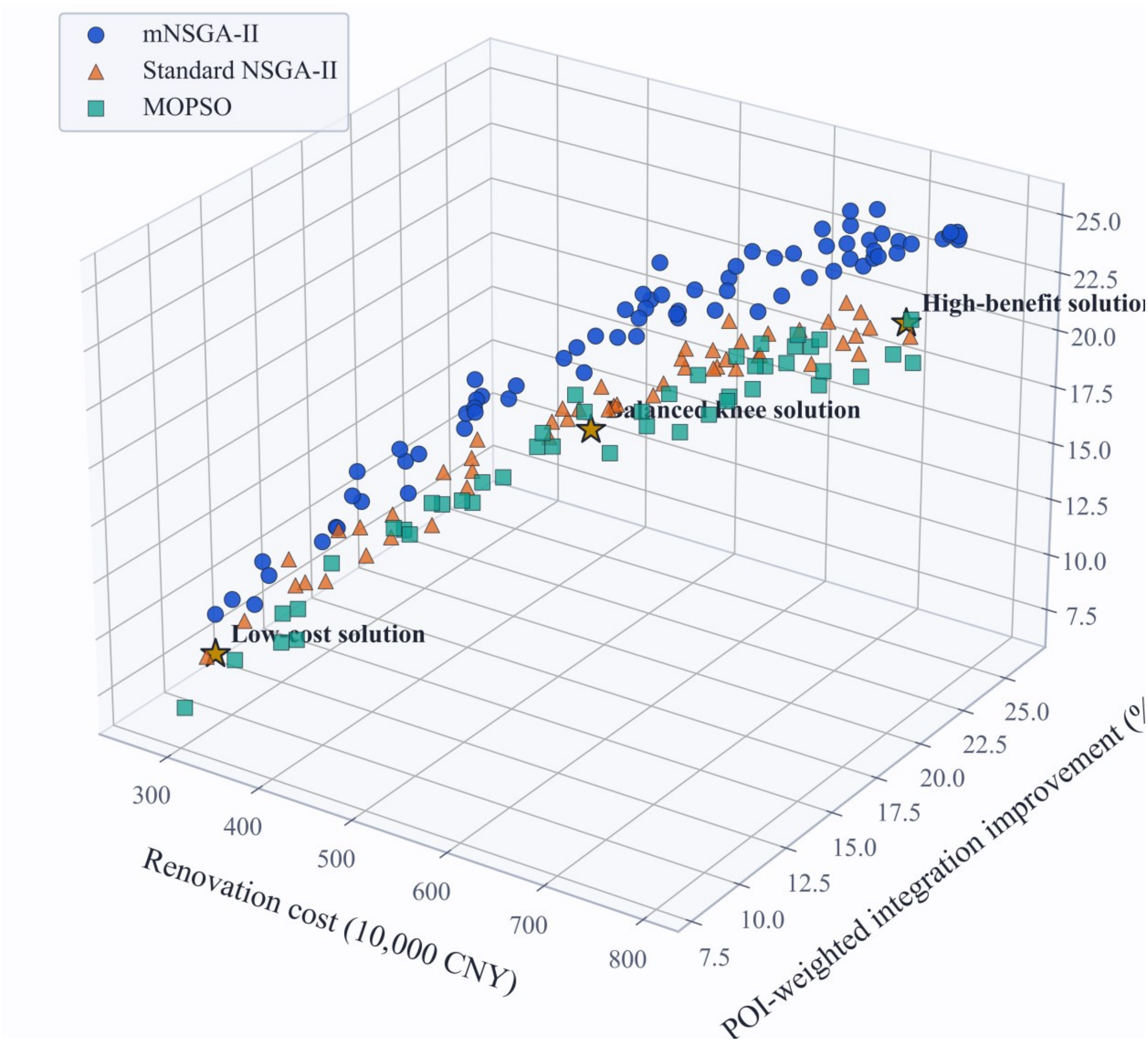

Figure 5. 3D Pareto front distribution of the three algorithms

In Figure 5, mNSGA-II has non-dominated solutions distributed in the low-cost area, medium budget area and high benefit area, and the coverage is larger than the two comparison algorithms. When the cost increases from 3 million yuan to about 5 million yuan, the integration degree and facility coverage increase rapidly; After the cost exceeds 6.5 million yuan, the frontier gradually flattens, indicating that the marginal benefit of continuing to increase investment declines. The knee points of the Pareto front are concentrated around 5-5.5 million yuan, which is suitable for the selection range of equilibrium schemes. The marginal benefit per unit cost is:

$$ME_k = \frac{\Delta F_k}{\Delta C} \tag{32}$$

Where ME_k is the marginal revenue of benefit index k; ΔF_k is the benefit increment in the adjacent budget interval; ΔC is the cost increment. When the cost is less than 5 million yuan, the increase of comprehensive benefit per million yuan is about 0.084; After exceeding 6.5 million yuan, it decreased to 0.027, a decrease of 67.9%.

4.4.3 Improved strategy ablation experiment

The demand stratification strategy, connectivity repair operator and POI gravity initialization are removed respectively, and the results are shown in Table 8.

Table 8. Ablation experiments of the mNSGA-II improved mechanism

Version of algorithm	IGD	HV	Feasible solution ratio	Group earnings gap	The first 50 generation HV
Complete mNSGA-II	0.0249	0.781	96.4%	0.084	0.672
Remove requirements stratification	0.0256	0.778	96.0%	0.147	0.669
Remove the repair operator	0.0331	0.739	69.8%	0.091	0.604
Remove the gravity initialization	0.0294	0.754	94.9%	0.088	0.571
Standard NSGA-II	0.0437	0.716	71.3%	0.162	0.523

After removing demand stratification, HV and IGD change relatively little, but the group payoff gap increases by 75.0%, indicating that the main contribution of demand stratification lies in improving the minimum payoff of the weak action group, rather than simply improving the overall goal. After removing the repair operator, the feasible solution rate decreases by 26.6 percentage points, which proves that the repair operator can significantly reduce budget overruns, road breaks, and measure conflicts. After removing the gravity initialization, HV decreases by 15.0% in the first 50 generations, indicating that this strategy mainly improves the convergence efficiency of the algorithm in the early stage.

4.5 Effectiveness test of the optimization scheme

4.5.1 Extraction of representative schemes

The low cost, equilibrium and high efficiency schemes are extracted from the non-dominated schemes obtained by mNSGA-II. The equilibrium scheme is determined by calculating the weighted distance from the scheme to the ideal point:

$$D_i^+ = \sqrt{\sum_{m=1}^{M} \omega_m \left(\hat{F}_{im} - F_m^+\right)^2} \quad (33)$$

Where D_i^+ is the distance between scheme i and the ideal point; $\hat{F}_{im}$ is the standardized target value; F_m^+ is the ideal value of the m-th objective; ω_m is the decision preference weight. The smaller the distance, the more balanced the scheme is between benefits and costs. The balanced solutions in Table 9 have similar costs to the empirical solutions, but their spatial combination methods differ.

Table 9. Composition of measures for representative optimization schemes

Scheme	The cost	Add or transform nodes	Widen road section	Add a new connection	The main strategy
Low-cost type	2.86 million yuan	At 12	Paragraph 7	Rule 2	Priority is given to eliminating inlet height difference and local bottlenecks
Type of equilibrium	5.23 million yuan	At 19	Paragraph 13	Rule 4	Connect the north side of the group and improve the barrier-free loop
High efficiency type	7.48 million yuan	At 27	Paragraph 19	Rule 6	Build a continuous barrier-free network across groups
Experience scheme	5.18 million yuan	At 16	Paragraph 15	Rule 2	Focus on widening the main road and adding rest facilities

The empirical scheme is more inclined to improve the current high-traffic main road, while the algorithm scheme adds facility entrance connection and edge group connection, indicating that the algorithm can identify a small number of measures with great structural effect based on the overall network relationship.

4.5.2 Index changes before and after optimization

The index improvement rate is:

$$IR_z = \frac{Z_{after} - Z_{before}}{Z_{before}} \times 100\% \quad (34)$$

In the formula, IR_z is the improvement rate of index Z; Z_{after} is the index value after optimization; Z_{before} is the status quo value. The balanced approach in Table 10 increased the weighted integration of POIs by 18.1%, the coverage of medical facilities by 16.8 percentage points, the coverage of living services by 13.4 percentage points, and the proportion of wheelchair-accessible road networks by 21.2 percentage points. Compared with the empirical scheme with similar costs, the balanced scheme has 5.9% higher weighted integration, 7.4 percentage points higher medical coverage, and 8.3 percentage points higher proportion of wheelchair accessible road networks.

Table 10. Comparison of key accessibility indicators before and after optimization

Scene	POI weights the degree of integration	Medical coverage rate	Life service coverage rate	Proportion of road network accessible by wheelchair	Continuous no rest distance
Status quo	0.426	62.8%	71.4%	68.5%	318 m
Low-cost type	0.468	70.3%	77.9%	78.6%	252 m
Type of equilibrium	0.503	79.6%	84.8%	89.7%	196 m
High efficiency type	0.526	84.1%	88.2%	95.3%	164 m
Experience scheme	0.475	72.2%	80.1%	81.4%	224 m

The index of the high-efficiency plan is the highest, but the cost increases by 43.0%, the weighted integration only further increases by 4.6%, and the medical coverage rate further increases by 4.5 percentage points compared with the balanced plan, indicating that its marginal revenue has decreased significantly. Therefore, under the general financial constraints, the balanced scheme has better benefit-cost coordination.

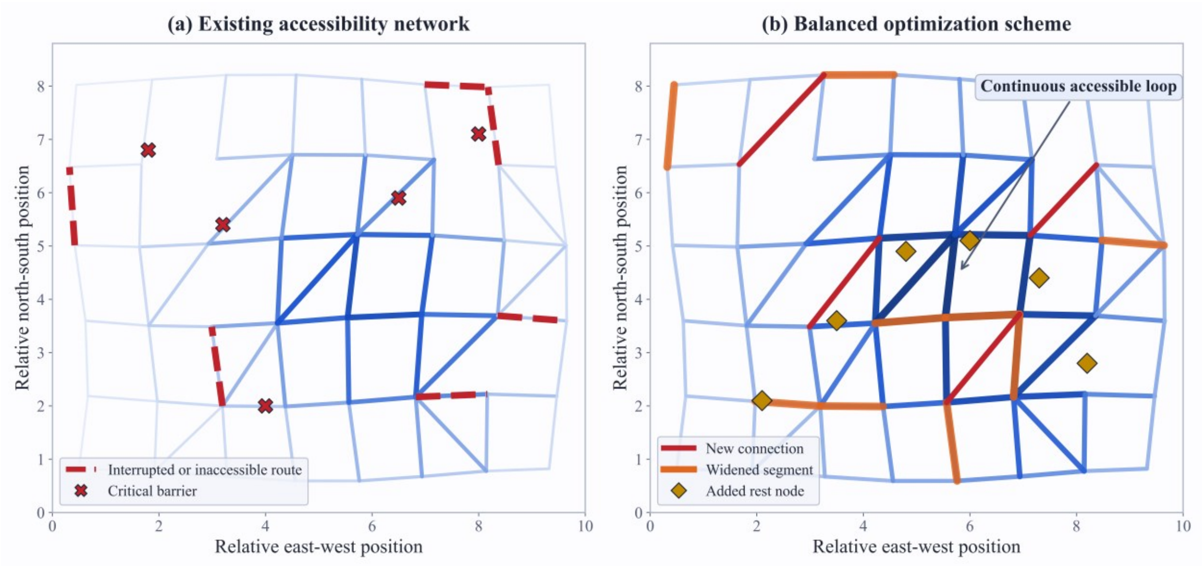

Figure 6. Comparison of barrier-free moving line before and after balanced scheme optimization

Figure 6 use left-right comparison. The left picture shows the current low integration area, wheelchair impassable road section and blind area of facilities and services; Figure 6 on the right shows the new connection, widened road section, ramp renovation and rest node. After optimization, a hierarchical network of "one continuous barrier-free main ring, two cross-group connections, and several branch lines of facility entrance" is formed. The residential group on the north side is connected to the service area of the center through a short connection, and the entrance of the activity room on the southwest side is connected to the wheelchair feasible network through ramps and widening measures.

4.5.3 Analysis of different budget scenarios

Budget ceilings of RMB3 million, RMB5 million, RMB7 million and RMB9 million were set respectively, and the results are shown in Table 11.

Table 11. Optimization results under different budget constraints

Budget cap	Weighted integration improvement rate	Improved medical coverage	Wheelchair road network improved	Unit one-million-yuan comprehensive benefit
3 million yuan	9.4%	7.8 percentage points	10.5 percentage points	0.086
5 million yuan	16.9%	14.9 percentage points	19.2 percentage points	0.079
7 million yuan	22.3%	20.1 percentage points	25.4 percentage points	0.061
9 million yuan	24.8%	22.7 percentage points	28.1 percentage points	0.044

Under the budget of 3 million yuan, the algorithm mainly selects low-cost measures such as step elimination, short bottleneck widening and rest node. After the budget reaches 5 million yuan, it can implement the connection project to change the road network structure, and the integration degree and facility coverage show a significant increase; When the budget increases from 7 million yuan to 9 million yuan, the weighted integration degree only increases by 2.5 percentage points, and the unit investment efficiency decreases by 27.9 percent.

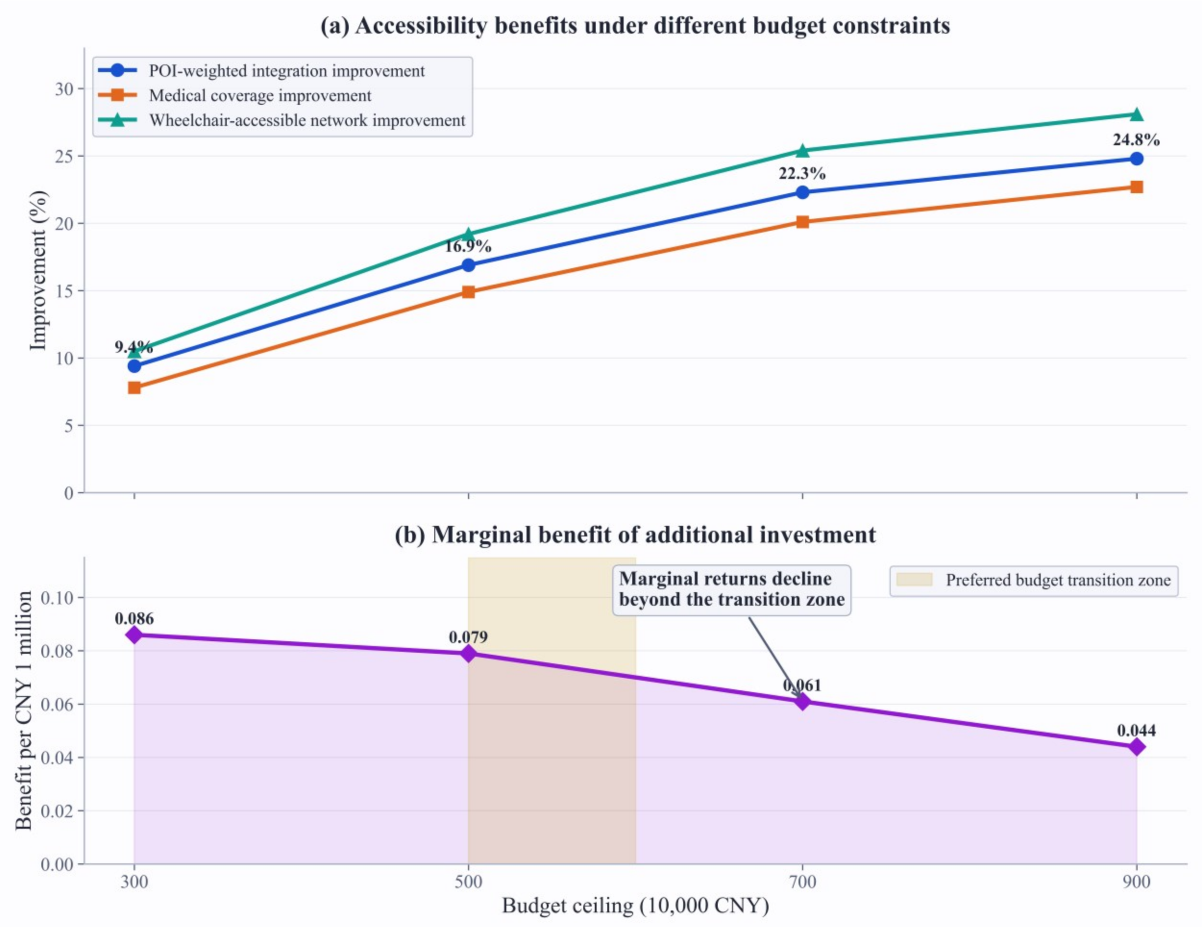

Figure 7. Comprehensive benefit and marginal revenue curves under different budget conditions

Figure 7 take budget as the horizontal axis, comprehensive accessibility improvement as the left vertical axis, and marginal revenue per unit cost as the right vertical axis. The comprehensive benefit increases with the increase of budget, but the slope of the curve decreases gradually; The marginal revenue shows an obvious turning point around 5 to 6 million yuan. This interval can be regarded as a priority budget range for the case community.

4.5.4 Expert evaluation and feedback from residents

Twelve experts in the fields of planning, landscape, transportation, rehabilitation and community governance were invited to conduct blind evaluation of the balanced algorithm scheme and the empirical scheme. Another 156 residents were invited to participate in the program evaluation, and 148 valid questionnaires were obtained. A 5-level Likert scale was used for evaluation, including continuity of movement lines, ease of facility arrival, applicability of weak action groups, feasibility of construction, and comprehensive acceptance. The reliability of the scale was tested by Cronbach's α coefficient:

$$\alpha = \frac{K}{K-1}\left(1 - \frac{\sum_{k=1}^{K} \sigma_k^2}{\sigma_T^2}\right) \tag{35}$$

Where α is the reliability coefficient of the scale; K is the number of items; σ_k^2 is the variance of the k-th item; σ_T^2 is the variance of the total score. The α coefficients of the expert and resident scales are 0.884 and 0.861 respectively, indicating that the scales have good internal consistency.

Table 12. Expert and resident evaluations of algorithmic schemes and empirical schemes

Dimension of evaluation	Algorithm scheme expert score	Experience program expert score	Algorithm scheme resident score	Experience program resident rating
Continuity of moving line	4.58	3.92	4.46	3.84
Facilities reach convenience	4.42	3.83	4.31	3.76
Weak action group applicability	4.67	3.58	4.39	3.61
Space and construction feasibility	4.08	4.25	4.02	4.09
Overall acceptance	4.36	3.97	4.28	3.83

The algorithm scheme is better than the empirical scheme in terms of continuity of movement line, convenience of facilities and applicability of weak action group, and the difference in the score of experts on applicability of weak action group reaches 1.09 points. The construction feasibility of the algorithm scheme is slightly lower, mainly because the new connection involves partial greening boundary adjustment and underground pipeline verification. This shows that the algorithm results can improve the efficiency of spatial optimization, but it still needs to go through property rights coordination, pipeline review and construction deepening.

The comprehensive acceptance of residents to the algorithm scheme was 4.28 points, 0.45 points higher than the empirical scheme. Low-activity and wheelchair-dependent residents showed higher support for the improvement of ramps, entrances and rest nodes, while some high-activity residents had concerns about reducing parking and adjusting green Spaces. Therefore, the spatial conflict should be reduced by combining parking reorganization and greening compensation in the implementation stage of the scheme.

4.5.5 Parameter sensitivity analysis

The POI weights, Gaussian decay coefficients, and structural contribution coefficients of medical and health care, life services, and social leisure were perturbed by ±10% and ±20%, respectively, and the Pareto scheme target values were recalculated. The elasticity of the index to the parameter is:

$$E_{Z,p} = \frac{\Delta Z/Z_0}{\Delta p/p_0} \tag{36}$$

Where, $E_{Z,p}$ is the elasticity coefficient of index Z to parameter p; Z_0 and p_0 are the benchmark index values and benchmark parameter values; ΔZ and Δp are the changes caused by parameter perturbations. Spearman correlation coefficient is used for the stability of scheme ranking:

$$\rho_s = 1 - \frac{6\sum_{i=1}^{n} d_i^2}{n(n^2-1)} \tag{37}$$

In the formula, ρ_s is the rank correlation coefficient between the benchmark scenario and the disturbance scenario; d_i is the ranking difference of scheme i in the two scenarios; n is the number of alternatives.

Table 13. Sensitivity analysis of key parameters

Parameters	Range of disturbance	The largest change in comprehensive accessibility	Lowest rank correlation coefficient	Sensitivity
Medical and health POI weight	±20%	6.8%	0.902	Medium
Life service POI weight	±20%	5.1%	0.927	Medium to low
Social leisure POI weights	±20%	3.6%	0.948	Be lower
Gaussian attenuation coefficient	±20%	7.4%	0.886	Relatively high
Structural contribution coefficient	±20%	6.2%	0.911	Msedium
Proportion of group population	±10%	4.3%	0.936	Be lower

The influence of Gaussian attenuation coefficient is the greatest, and the maximum change of comprehensive accessibility by ±20% disturbance is 7.4%, and the lowest ranking correlation coefficient is 0.886. The POI weight of medical health has the second highest impact, indicating that the number of medical facilities is small and the spatial distribution is uneven, and changes in its weight will significantly change the priority of connectivity measures.

The ranking correlation coefficients of all disturbance scenarios are higher than 0.88, and the balanced schemes are always in the range of the top 5% of non-dominated schemes, indicating that the core conclusions have good robustness.

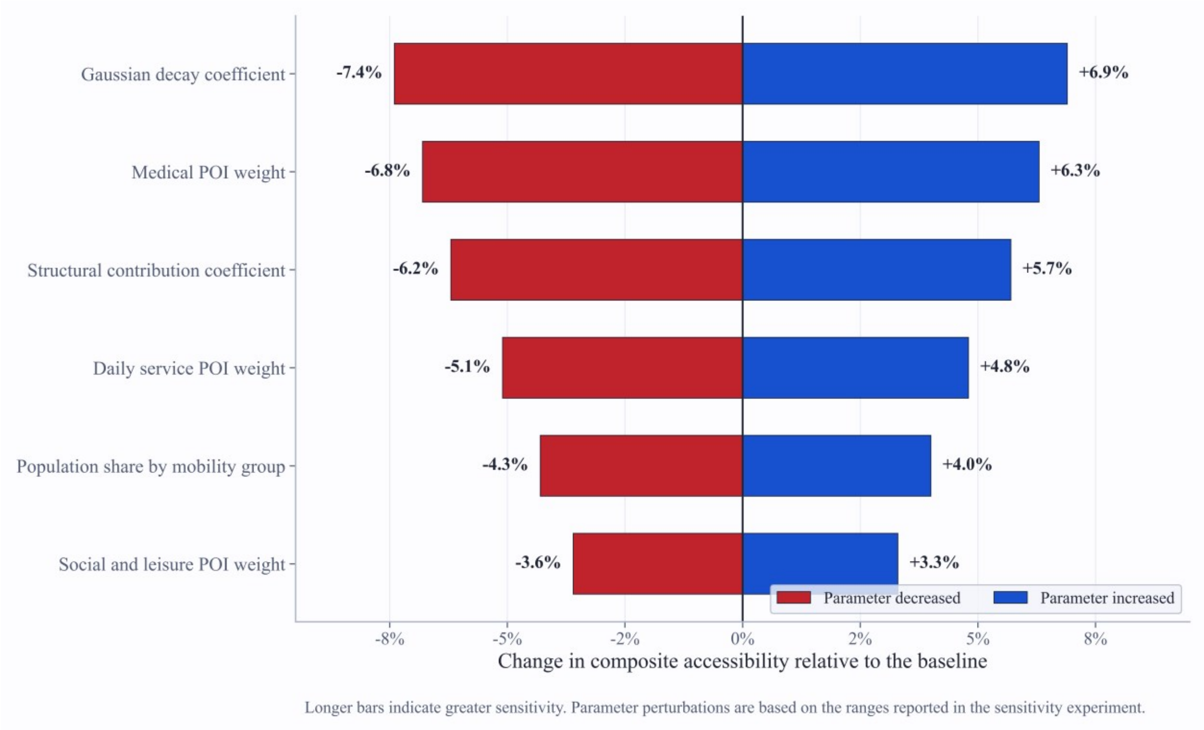

Figure 8. Tornado diagram for sensitivity analysis of key parameters

In Figure 8, the comprehensive accessibility change rate is used as the horizontal axis, and the parameters are arranged from high to low according to the degree of influence. The Gaussian decay coefficient and the medical health POI weight correspond to the longest horizontal bars, while the social leisure weight and the group population proportion correspond to the shorter horizontal bars. The results show that the travel trajectory and questionnaire data should be used first to calibrate the attenuation parameters in practical research, rather than directly applying the empirical values of other communities.

4.5.6 Spatial fairness test

In order to avoid the overall benefit masking the adverse situation of the marginal group, the Gini coefficient of residential group accessibility was used to evaluate spatial equity. The Gini coefficient of accessibility of the current eight groups is 0.286, and it drops to 0.243, 0.196, 0.174 and 0.231 for the low-cost, balanced, high-efficiency and empirical schemes, respectively. The equity improvement rate is:

$$ER = \frac{G_0 - G_1}{G_0} \times 100\% \tag{38}$$

Where ER is the improvement rate of spatial equity; G_0 is the Gini coefficient of group accessibility before optimization; G_1 is the optimized Gini coefficient.

The equity improvement rate of the balanced scheme is 31.5 percent, which is higher than 19.2 percent of the empirical scheme. The composite index for the least accessible group increased from 0.308 to 0.447, an increase of 45.1%. This shows that the improved algorithm not only improves the overall accessibility of the community but also improves the service conditions of the marginal area and the group with weak mobility.

5. CONCLUSIONS

This study constructs a barrier-free route research framework integrating POI data, space syntax, hierarchical elderly needs, and multi-objective optimization, addressing the limitations of traditional community aging evaluations that rely on static spatial descriptions and separate road-structure from facility-function analyses. The results demonstrate that road topology alone inadequately explains elderly travel behavior. By incorporating the importance, service capacity, and distance-decay effects of medical, daily service, and social-leisure facilities into space syntax, the model accurately identifies alignments or mismatches between structural centrality and functional service centers. Further integration of walking speed, slope tolerance, continuous walking distance, rest needs, and visual continuity deepens accessibility evaluation from "whether roads are spatially connected" to "whether different elderly groups can travel safely, continuously, and purposefully." Case validation confirms that the POI-weighted model and multi-level modification framework better explain observed elderly travel patterns, particularly for low-activity and wheelchair-dependent groups, proving that facility attractiveness and group-specific behavioral constraints are indispensable components of community accessibility assessment.

In optimization, node addition, road widening, and breakpoint connection are encoded as computable renovation variables within an improved multi-objective NSGA-II that simultaneously maximizes POI-weighted integration, expands facility coverage, and minimizes cost. The demand-stratified Pareto strategy prevents overall average benefits from masking weak-mobility group needs; the spatial connectivity repair operator eliminates isolated nodes, invalid connections, and measure conflicts; and POI-gravity-based initialization guides the algorithm toward areas with high facility demand but insufficient current accessibility. The resulting Pareto frontier offers effective trade-offs among accessibility improvement, facility coverage enhancement, and construction cost across different budget levels, producing low-cost, balanced, and high-efficiency schemes adaptable to varied fiscal and renovation objectives. For community aging design, priority should be given to ensuring continuous connections between residential entrances, main walking passages, and high-frequency facilities, followed by bottleneck widening, breakpoint connection, ramp improvement, and rest-node supplementation, avoiding the dispersion of limited funds across localized measures lacking structural impact.

Methodologically, this study systematically integrates spatial structure, facility function, group behavior, and design optimization. The POI-weighted space syntax model transcends the traditional assumption of homogeneous road nodes by embedding facility category weights, service capacity, accessibility quality, and distance decay into network analysis, expanding syntactic indices from mere road centrality to functional accessibility reflecting age-friendly service opportunities. The hierarchical needs matrix incorporates facility preferences and access constraints of high-activity, low-activity, and wheelchair-dependent groups, avoiding accessibility overestimation from uniform walking radii and average behavioral parameters. The improved NSGA-II transforms spatial evaluation into implementable measure combinations, handles group equity through hierarchical Pareto sorting, ensures topological and engineering legality via connectivity repair, and enhances search efficiency through POI-gravity guidance. These advances elevate community aging research from static evaluation to a computational design process with explicit objectives, measure coding, and scheme comparison capabilities. At the application level, the workflow—encompassing data collection, status evaluation, shortfall diagnosis, optimization, scheme screening, and implementation feedback—serves both pre-renewal diagnosis and post-implementation performance assessment, providing a common quantitative basis for planners, community managers, and residents. However, algorithm results remain decision-support tools; final plans must be refined considering property boundaries, underground utilities, fire safety, construction logistics, and resident preferences to effectively bridge computational outputs with design practice.

Several limitations remain. Multi-source POI data may suffer from inconsistent category standards, location offsets, facility omissions, and delayed updates, while elderly survey and trajectory samples are constrained by survey periods, sample size, device usability, and privacy requirements. The model primarily represents outdoor walking spaces as two-dimensional segment networks, excluding internal corridors, elevators, staircases, connecting bridges, and underground spaces, thus incompletely capturing the full journey from residential units to facility service points. Facility attractiveness and road attributes are based on static data, not yet reflecting temporal variations in opening hours, service queueing, temporary occupancy, weather conditions, or pedestrian congestion. Future work will integrate dynamic data sources (mobile positioning, wearable devices, environmental sensors) to establish time-varying POI and path impedance models; combine BIM with GIS to construct multi-layer three-dimensional networks incorporating outdoor roads, building entrances, indoor corridors, and vertical circulations; and develop dynamic optimization methods accommodating facility schedule changes, phased construction, and uncertainty constraints with robust optimization and real-time feedback. Cross-case validation across diverse communities will further generalize the framework, progressively building a sustainable aging-adaptation decision platform responsive to evolving facility status, heterogeneous group needs, and changing implementation conditions.

Abbreviations

POI, Point of Interest;

NSGA-II, Nondominated Sorting Genetic Algorithm II;

mNSGA-II, improved Nondominated Sorting Genetic Algorithm II;

MOPSO, Multi-Objective Particle Swarm Optimization;

GD, Generational Distance;

IGD, Inverted Generational Distance;

HV, Hypervolume;

AHP, Analytic Hierarchy Process;

PWI, POI-Weighted Integration;

AAI, Accessibility Index;

SP, Spacing Index;

SMR, Spatial Matching Rate;

IR, Improvement Rate;

ER, Equity Improvement Rate;

CAD, Computer-Aided Design;

GIS, Geographic Information System;

BIM, Building Information Modeling;

OpenStreetMap, OpenStreetMap;

QGIS, Quantum Geographic Information System;

MAE, Mean Absolute Error;

R^2, Coefficient of Determination;

GPU, Graphics Processing Unit;

CPU, Central Processing Unit.

Supplementary Material

Not applicable.

Appendix

Not applicable.

Ethics approval and consent to participate.

This study did not involve human participants, animal subjects, or any data requiring ethical approval. Therefore, ethics approval and consent to participate are not applicable.

Acknowledgements

The authors would like to thank the editors of this journal and all the anonymous reviewers who provided valuable comments on this work.

Competing interests

The authors declare that they have no financial or personal relationships that may have inappropriately influenced them in writing this article.

Author contributions

All authors have read and agreed to the published version of the manuscript. The author's contributions are specified as follows: **J.Z.:** Conceptualization, Methodology, Software, Validation, Formal analysis, Investigation, Resources, Data Curation, Writing – original draft, Writing – review & editing, Visualization, Supervision, Project administration.

Funding information

The authors declare that no funds, grants, or other support were received during the preparation of this manuscript.

Data availability

The data that support the findings of this study are available upon request from the corresponding authors, **J.Z.**

Disclaimer

The views and opinions expressed in this article are those of the authors and are the product of professional research. It does not necessarily reflect the official policy or position of any affiliated institution, funder, agency, or that of the publisher. The authors are responsible for this article's results, findings, and content.

Declaration of AI and AI-assisted Technologies in the Writing Process

During the writing of this article, the author used ChatGPT for spelling and grammar checking. After using this tool, the author reviewed and edited the content as needed and assumes full responsibility for the final published content.

REFERENCES

[1] Miano, A., Civera, M., Aloschi, F., De Biagi, V., Chiaia, B., Parisi, F., & Prota, A. (2024). Efficiency assessment of urban road networks connecting critical node pairs under seismic hazard. *Sustainability*, *16*(17), 7465. https://doi.org/10.3390/su16177465

[2] Yang, J., Zhang, J., & Song, L. (2026). Construction Risk Measurement and Driving Mechanisms in Old Residential Community Renovation Projects: A Combined Correlation–SEM Approach. *Buildings*, *16*(14), 2740. https://doi.org/10.3390/buildings16142740

[3] Peng, W., Xia, Y., Han, Y., Wang, H., Tang, Y., Liu, X., & Chen, Y. (2026). Research on Earthquake Demolition Rescue Robot Design Based on UXM–Kano–QFD Framework. *Applied Sciences*, *16*(9), 4456. https://doi.org/10.3390/app16094456

[4] Nguyen, P. H. (2023). A fully completed spherical fuzzy data-driven model for analyzing employee satisfaction in logistics service industry. *Mathematics*, *11*(10), 2235. https://doi.org/10.3390/math11102235

[5] Chin, K. S., Lo, K. C., & Leung, J. P. (2010). Development of user-satisfaction-based knowledge management performance measurement system with evidential reasoning approach. *Expert Systems with Applications*, *37*(1), 366-382. https://doi.org/10.1016/j.eswa.2009.05.051

[6] Liu, X., Lv, Y., Li, W., Peng, L., & Wu, Z. (2025). Assessment of Age-Friendly Streets in High-Density Urban Areas Using AFEAT, Street View Imagery, and Deep Learning: A Case Study of Qinhuai District, Nanjing, China. *Buildings*, *15*(19), 3518. https://doi.org/10.3390/buildings15193518

[7] Wang, X., & Yin, P. (2026). From Facility Agglomeration to Service Accessibility: A Spatial Mismatch Analysis of Elderly Care and Residential Spaces in the 15-Minute Life Circle for Sustainable Aging—A Case Study of Zhifu District, Yantai. *Sustainability*, *18*(14), 6962. https://doi.org/10.3390/su18146962

[8] Wang, Y., Shen, Y., Zhang, X., Cui, G., & Sun, J. (2018). An improved non-dominated sorting genetic algorithm-II (INSGA-II) applied to the design of DNA codewords. *Mathematics and Computers in Simulation*, *151*, 131-139. https://doi.org/10.1016/j.matcom.2018.03.011

[9] Zhang, Y., Dai, W., Xu, M., Zou, J., Zhang, X., & Xiong, H. (2019). Depth estimation from light field using graph-based structure-aware analysis. *IEEE Transactions on Circuits and Systems for Video Technology*, *30*(11), 4269-4283. https://doi.org/10.1109/TCSVT.2019.2954948

[10] Meng, Z., Yıldız, B. S., Li, G., Zhong, C., Mirjalili, S., & Yildiz, A. R. (2023). Application of state-of-the-art multiobjective metaheuristic algorithms in reliability-based design optimization: a comparative study. *Structural and Multidisciplinary Optimization*, *66*(8), 191. https://doi.org/10.1007/s00158-023-03639-0

[11] da Silva, M. A., Garcia, R. D. P., & Carlo, J. C. (2026). Multi-objective optimization algorithms for building performance assessment–A benchmark. *International Journal of Architectural Computing*, *24*(1), 35-59. https://doi.org/10.1177/14780771241296263

[12] Kumari, R., Kumar, D., & Kumar, V. (2017). A conceptual comparison of NSGA-II, OMOPSO and AbYss algorithms. *International Journal of Internet Technology and Secured Transactions*, *7*(4), 330-352. https://doi.org/10.1504/IJITST.2017.091520

[13] Liu, A. H., Ellul, C., & Swiderska, M. (2021). Decision making in the 4th dimension—Exploring use cases and technical options for the integration of 4D BIM and GIS during construction. *ISPRS International Journal of Geo-Information*, *10*(4), 203. https://doi.org/10.3390/ijgi10040203

[14] Le, T., Hassan, F., Le, C., & Jeong, H. D. (2022). Understanding dynamic data interaction between civil integrated management technologies: a review of use cases and enabling techniques. *International Journal of Construction Management*, *22*(6), 1011-1032. https://doi.org/10.1080/15623599.2019.1678863

[15] Hu, D., Zhu, L., & Wei, J. (2026). Chinese vernacular villages renovation: A methodology for establishing a 3D interactive database. *Journal of Cultural Heritage*, *78*, 67-78. https://doi.org/10.1016/j.culher.2026.01.004

[16] Rathi, G., Kamble, S., & Sharma, N. (2026). Road Traffic Outlier Detection for Reliable ITS: A Multi-Level Framework from Point to Network Fidelity. *IETE Technical Review*, *43*(2), 204-221. https://doi.org/10.1080/02564602.2025.2608748

[17] Geremew, G. (2026). Modeling and analyzing the impact of on-street parking on traffic flow: a study of the main highway in Debre Markos Town, Ethiopia. *Transportation*, *53*(2), 783-817. https://doi.org/10.1007/s11116-024-10513-5

[18] Fellendorf, M., & Vortisch, P. (2010). Microscopic traffic flow simulator VISSIM.

In *Fundamentals of traffic simulation* (pp. 63-93). New York, NY: Springer New York. https://doi.org/10.1007/978-1-4419-6142-6_2

[19] Chen, C. Y., Hong, I. H., Chen, R. C., Chang, W. T., & Chang, C. C. (2025). A robust Pareto model for electric vehicle charging station deployment in urban areas considering psychology effects of drivers. *International Journal of Production Research*, *63*(10), 3564-3588. https://doi.org/10.1080/00207543.2024.2424975

[20] Bao, Q., Gao, M., Chen, J., & Tan, X. (2024). Location and size planning of charging parking lots based on EV charging demand prediction and fuzzy bi-objective optimization. *Mathematics*, *12*(19), 3143. https://doi.org/10.3390/math12193143

[21] Yang, C., Zhao, M., Wang, C., Deng, K., Jiang, L., & Xu, Y. (2020). Urban road DEM construction based on geometric and semantic characteristics. *Earth Science Informatics*, *13*(4), 1369-1382. https://doi.org/10.1007/s12145-020-00510-4

[22] Yue, L., & Wang, H. (2019). An optimization design method of combination of steep slope and sharp curve sections for mountain highways. *Mathematical Problems in Engineering*, *2019*(1), 2416342. https://doi.org/10.1155/2019/2416342

[23] Hu, Y., Tang, X., Wang, Y., & Chen, J. (2026). Quantifying informal street vendors clusters through geo-spatial indicators and geo-tagged social media: a socio-spatial fusion approach for human-centered urban renewal. *Journal of Asian Architecture and Building Engineering*, 1-25. https://doi.org/10.1080/13467581.2026.2652689

[24] Pang, R., Xiao, J., Yang, J., & Sun, W. (2025). Spatial distribution characteristics and influencing factors of public service facilities for children—a case study of the central urban area of Shenyang. *Land*, *14*(7), 1485. https://doi.org/10.3390/land14071485

[25] Zhang, N., Wang, S., Liang, H., Huang, Z., Li, X., & Wang, Z. (2025). Heterogeneity analysis of resident demands and public service facilities in megacities of China from the perspective of urban health examination. *ISPRS International Journal of Geo-Information*, *14*(5), 188. https://doi.org/10.3390/ijgi14050188

[26] Han, M., Xu, S., Zhou, Z., & Wang, J. (2025). Constructing an urban spatial resilience assessment framework based on public service facilities: a case study of Beijing. *Clean Energy and Sustainability*, *3*(1), 10001. https://doi.org/10.70322/ces.2025.10001

[27] Wang, Z., Zhang, Z., Su, T., Ding, Z., & Zhao, T. (2024, December). Research on supply chain network optimisation based on the CNNs-BiLSTM model. In *2024 International Conference on Information Technology, Comunication Ecosystem and Management (ITCEM)* (pp. 197-202). IEEE. https://doi.org/10.1109/ITCEM65710.2024.00044

[28] Zhao, T., Chen, G., Pang, C., Seenoi, P., Papukdee, N., Busababodhin, P., & Du, Y. (2025). Hybrid convolutional neural network-graph attention network-gradient boosting decision tree model for seismic impedance inversion prediction. *J Seismic Explor*, *34*(5), 81-98. https://doi.org/10.36922/JSE025310051

[29] Zhao, T., Chen, G., Pang, C., Li, L., & Busababodhin, P. (2026). Forecasting global agricultural trade imbalances using a hybrid deep learning and gradient boosting framework. *Discover Computing*, *29*(1), 443. https://doi.org/10.1007/s10791-026-10367-8

[30] Liu, Y., Gong, M., Chen, G., & Zhao, T. (2025, July). CNN-LSTM-based spatio-temporal prediction model for photovoltaic power generation. In *Proceedings of the 2025 2nd International Conference on Big Data and Digital Management* (pp. 570-575). https://doi.org/10.1145/3768801.3768892

[31] Zhao, T., Chen, G., & Busababodhin, P. (2026). An intelligent expert system for logistics disruption prediction and mitigation in global supply chains: Integrating graph-based risk inference with ensemble forecasting. *Scientific Reports*. https://doi.org/10.1038/s41598-026-61617-0

[32] Peng, M., Hu, J., & Zhao, T. (2026, March). Hybrid ARIMA-LSTM model for international trade logistics demand forecasting. In *IET Conference Proceedings CP982* (Vol. 2026, No. 9, pp. 243-247). Stevenage, UK: The Institution of Engineering and Technology. https://doi.org/10.1049/icp.2026.2978

[33] Du, Y., Chen, G., Pang, C., & Zhao, T. (2025). Prediction of fracture and vug parameters in carbonate reservoirs using a combined T-GNO-PINN approach. *Journal of Seismic Exploration*, *35*(1), 46. https://doi.org/10.36922/JSE025330057

[34] Zhang, Z., Jia, Z., Wei, J., Xiao, Y., Zhang, R., & Zhao, T. (2025, June). Combining 5G Communication Technology with XGboost Model for Global Gas Trade Flow Prediction. In *International Conference on Artificial Intelligence and Communication Technology* (pp. 53-64). Cham: Springer Nature Switzerland. https://doi.org/10.1007/978-3-032-06376-2_5

[35] Zhang, Z., Qiu, T., Liao, Z., Liu, H., Wei, C., & Zhao, T. (2025, July). Research on global power equipment trade prediction and logistics optimization based on 5G and edge computing. In *International Conference on Optoelectronics and Information Technology (ICOIT 2025)* (Vol. 13665, pp. 302-310). SPIE. https://doi.org/10.1117/12.3071144

[36] Wang, A., Chen, G., Pang, C., & Zhao, T. (2025, July). Research on the prediction of telecommunication fraud using BKA-CNN-LSTM model from the perspective of big data. In *Proceedings of the 2025 2nd International Conference on Big Data and Digital Management* (pp. 576-582). https://doi.org/10.1145/3768801.3768893

[37] Wang, Z., Wan, Y., Chen, G., Li, M., Tang, J., & Zhao, T. (2025, June). Multiscale Time Series Prediction of Crude Oil Prices Based on Transformer and CNN. In *International Conference on Artificial Intelligence and Communication Technology* (pp. 430-443). Cham: Springer Nature Switzerland. https://doi.org/10.1007/978-3-032-06372-4_36

[38] Chen, G., Zhao, T., Busababodhin, P., & Jin, Y. (2023, July). Combined Prediction Model of Gasoline Octane Loss Value Based on XGboost-GBDT Combined Prediction. In *2023 7th International Conference on Computer, Software and Modeling (ICCSM)* (pp. 42-46). IEEE. https://doi.org/10.1109/ICCSM60247.2023.00017

[39] Zhao, T., & Xu, H. (2025). A Novel STCA-LightGBM-SVR Hybrid Model for Port Cargo Throughput Prediction. In *Artificial Intelligence and Applications*. https://doi.org/10.47852/bonviewAIA62027055

APA Citation

Zhang, J. (2026). Optimization Model for Barrier Free Accessible Routes in Community Age Friendly Environment Design Based on POI and Space Syntax. *Journal of Discovery Core, 1*(1), 129-162. **https://doi.org/10.67541/jdc2606**